SPACE RESEARCH COORDINATION CENTER

TEMPERATURE DISTRIBUTION AND THE LOCATION OF THE SOLIDUS, MUSHY AND LIQUIDUS ZONES FOR BINARY ALLOYS IN REMELTING PROCESSES

BY

L. FERNANDO CARVAJAL AND

G. E. GEIGER

DEPARTMENT OF MECHANICAL ENGINEERING

SRCC REPORT NO. 118

NGL-39-011-002

UNIVERSITY OF PITTSBURGH

PITTSBURGH, PENNSYLVANIA

9 FEBRUARY 1970

The Space Research Coordination Center, established in May, 1963, has the following functions: (1) it administers predoctoral and postdoctoral fellowships in space-related science and engineering programs; (2) it makes available, on application and after review, allocations to assist new faculty members in the Division of the Natural Sciences and the School of Engineering to initiate research programs or to permit established faculty members to do preliminary work on research ideas of a novel character; (3) in the Division of the Natural Sciences it makes an annual allocation of funds to the interdisciplinary Laboratory for Atmospheric and Space Sciences; (4) in the School of Engineering it makes a similar allocation of funds to the Department of Metallurgical and Materials Engineering and to the program in Engineering Systems Management of the Department of Industrial Engineering; and (5) in concert with the University's Knowledge Availability Systems Center, it seeks to assist in the orderly transfer of new space-generated knowledge in industrial application. The Center also issues periodic reports of space-oriented research and a comprehensive annual report.

The Center is supported by an Institutional Grant (~~NsG-116~~) from the National Aeronautics and Space Administration, strongly supplemented by grants from the A. W. Mellon Educational and Charitable Trust, the Maurice Falk Medical Fund, the Richard King Mellon Foundation and the Sarah Mellon Scaife Foundation. Much of the work described in SRCC reports is financed by other grants, made to individual faculty members.

TEMPERATURE DISTRIBUTION AND THE LOCATION OF THE SOLIDUS, MUSHY AND LIQUIDUS ZONES FOR BINARY ALLOYS IN REMELTING PROCESSES

by

L. FERNANDO CARVAJAL

and

G. E. GEIGER

DEPARTMENT OF MECHANICAL ENGINEERING

UNIVERSITY OF PITTSBURGH

ABSTRACT

The solidification of a binary alloy in a remelting process is considered. The temperature distribution in an ingot in quasi-steady state in a externally cooled cylindrical mold is determined, from which the liquidus, mushy and solidus regions are found. Normal non-equilibrium solidification is assumed. Curves are presented for aluminum -4.5% copper alloy system.

NOMENCLATURE

Roman letters

a	constant	
C_S	average concentration of solute in solid weight percent	
C_L	average concentration of solute in liquid weight percent	
c_S	specific heat of solid	(cal/gr^oC)
c_L	specific heat of liquid	(cal/gr^oC)
c	specific heat and expression defined in eq. (19)	(cal/gr^oC)
c_w	specific heat of water	(cal/gr^oC)
D_w	crucible channel width	(cm)
d_m	mold thickness	(cm)
d_g	gap thickness	(cm)
d_s	slag skin thickness	(cm)
f_S	fraction of solid	
f_L	fraction of liquid	
H_T	enthalpy of the alloy	(cal/gr)
H_S	enthalpy of the solid phase	(cal/gr)
H_S', H_S''	enthalpy of the components of the solid phase, solute and solvent	(cal/gr)
H_L	enthalpy of the liquid phase	(cal/gr)
H_L', H_L''	enthalpy of the components of the liquid phase, solute and solvent	(cal/gr)
h	total heat transfer coefficient	(cal/sec cm^2 ^oC)

h'	total heat transfer coefficient including radiation effects	(cal/sec cm^2 ^oC)
h_w	mold to water convection factor	(cal/sec cm^2 ^oC)
H_{MS}	heat of mixing in the solid	(cal/gr)
H_{ML}	heat of mixing in the liquid	(cal/gr)
K	scale constant	
K_1	parameter equal to RU	(cm^2/sec)
K_2	parameter equal to RH_{max}	(cal/sec cm ^oC)
k	thermal conductivity	(cal/sec cm ^oC)
k_S	solid thermal conductivity	(cal/sec cm ^oC)
k_L	liquid thermal conductivity	(cal/sec cm ^oC)
k_g	thermal conductivity in the gap between mold and ingot	(cal/sec cm ^oC)
k_m	thermal conductivity of the mold	(cal/sec cm ^oC)
m_L	slope of the liquidus line	
R	radius of the ingot	(cm)
r	radial coordinate	dimensionless
r'	radial coordinate	(cm)
T	temperature	(^oC)
T_M	melting point temperature of pure solvent	(^oC)
T_L	liquidus temperature of alloy	(^oC)

T_S	solid line (or eutectic) temperature	(^oC)
T_{slag}	the maximum temperature of ingot at center of surface in contact with slag	(^oC)
T_w	cooling water temperature	(^oC)
t	time	
U	speed of progress of the melt	(cm/sec)
v_T	specific volume of the alloy	(cm^3/gr)
v_S	specific volume of the solid phase	(cm^3/gr)
v_L	specific volume of the liquid phase	(cm^3/gr)
V_w	water velocity in mold	(cm/sec)
x	transformed z coordinate	
z	axial coordinate	dimensionless
z'	axial coordinate	(cm)
z_I	length of the ingot	dimensionless
z_S	depth of the solid line	dimensionless
z_L	depth of the liquid line	dimensionless

Greek letters

ϵ	interchange factor for radiation	
μ_w	viscosity of water	(gr/sec cm)
Θ	Transform of the temperature defined in eq. (17)	
ρ	density of the alloy	(gr/cm^3)
ρ_w	density of the water	(gr/cm^3)
σ	Stefan-Boltzman constant	(cal/sec $cm^2 {}^oC^4$)

INTRODUCTION

The solidification of a binary alloy, such as aluminum -4.5% copper, is considered in the electroslag remelting process. This process is closely related to the continuous casting process, but differs in that the velocity of growth of the ingot is not of such a magnitude greater than the velocity of the solidifying front to allow the heat transfer to be treated as one dimensional. Also since alloy solidification is considered, a third region, "the mushy zone", is introduced, in addition to the solid and liquid regions.

The solidification of a pure metal in vaccum arc melting for two dimensional transient heat flow using an explicit finite difference numerical method was considered by Manior and Pierce (1). Wood (2) proposed semi-analytically derived expressions for the shape of the solid-liquid interface for the same case. A study of the thermal equilibrium associated with the process is given by Rossin (3). Experimental studies to determine the shape of the liquid pool have been made by Bungardt and Tromel (4) and by Beall, et. al. (5)(6). Recently Patel and Boley (7) did an analytical study which included imperfect mold contact.

Alloy solidification studies from the heat transfer point of view have been made by Tien (8), Tien and Geiger (9)(10) and by Koump, Tien and Kim (11). The process of electroslag remelting is described by Bhat (12).

STATEMENT OF PROBLEM

The electroslag remelt process consists of an electrode, of any size and shape, melted into a water cooled crucible. The liquid metal that forms at the top of the electrode falls to the bottom of the crucible and feeds a growing ingot. The electric current flows between the electrode and the crucible through a molten flux or slag, which always remains at the top of the ingot, covering part of the electrode. The slag excludes the outer atmosphere from the liquid metal, and also aids in refining the metal. Heat is withdrawn by a water cooled crucible. The rate of heat production and slag temperature determine the solidification process. A fast rate of melting will cause a deeper liquid pool in the ingot which will in turn tend to produce radially oriented grain-growth, while a slow melting rate produces grains which are more axially oriented.

Bungardt and Tromel (4) and Clites and Beall (13) show from experimental work in vacuum-arc melting that the liquid pool shape remains fairly constant after the ingot length is more than one diameter. This should also be the case for electroslag remelting where the heat of dissipation is more uniform and stable.

In the ingot the latent heat of solidification is released in a mushy zone between the liquid and solid regions, since solidification takes place in a definite

range of temperatures.

The object here is to determine from the temperature distribution in a cylindrical ingot the shape of the respective zones when the process reaches a quasi-steady state condition.

PROPERTIES

The liquid and solid phases of a binary alloy can coexist in equilibrium at different temperatures depending on the composition of the phases and, in general, the portion of solid just frozen has a different composition than the liquid from which it came. This affects the concentration in both the remaining liquid and solid, and requires that a different value of temperature of equilibrium be maintained.

For phase diagrams with linear solidus and liquidus lines, the solid fraction f_S for the "normal non-equilibrium solidification" is shown by Pfann (14) to be:

$$f_S = 1 - \left(\frac{T_M - T_L}{T_M - T}\right)^{\frac{1}{1-C_{S/C_L}}} \qquad \text{(Eq. 1)}$$

The equilibrium partition ratio, C_{S/C_L}, is a constant in this case. Note that when T equals T_S, f_S is still positive, and equation (1) is no longer valid. The remaining liquid solidifies isothermally since its composition is the eutectic, and thus a discontinuity occurs in the heat release.

Dendritic growth will be assumed in the mushy zone. The dendrites can be considered as extending from the solid to the liquid phase (11)(15)(16). The temperature at the top of the dendrite is the liquidus one corresponding to the alloy and the temperature in the base is that of the eutectic.

Most of the data for alloys reported in the literature is for the solid state and then only for a discreet number of compositions. The properties of specific volume and specific heat of an alloy and its composition approaches linearity closely enough so that these properties can be calculated directly from the contribution of the components. The following equations were constructed from data given in references (17), (18) and (19). For the specific volume of aluminum

$$v_{S_{Al}} = 0.3706 + 0.39 \cdot 10^{-4}(T-25) \qquad \text{(Eq. 2)}$$

$$v_{L_{Al}} = 0.4007 + 0.39 \cdot 10^{-4}(T-25) \qquad \text{(Eq. 3)}$$

For the specific volume of copper

$$v_{S_{Cu}} = 0.1161 + 0.0416 \cdot 10^{-4}(t-25) \qquad \text{(Eq. 4)}$$

$$v_{L_{Cu}} = 0.1216 \qquad \text{(Eq. 5)}$$

The alloy specific volume is then calculated from

$$v_T = v_{Al} - (v_{Al} - v_{Cu})C_{Cu} \qquad \text{(Eq. 6)}$$

The specific heats of aluminum can be given as

$$c_{S_{Al}} = 0.215 + 2(0.551 \cdot 10^{-4})(T-25) \qquad \text{(Eq. 7)}$$

$$c_{L_{Al}} = 0.259 \qquad \text{(Eq. 8)}$$

The specific heats of copper are

$$c_{S_{Cu}} = 0.092 + 2(0.1087 \cdot 10^{-4})(T-25) \qquad \text{(Eq. 9)}$$

$$c_{L_{Cu}} = 0.118 \qquad \text{(Eq. 10)}$$

The specific heat of the alloy can be calculated as the derivative of the enthalpy of the alloy with respect to the temperature. The enthalpy is determined by adding the contributions of the components, the heat of mixing and the possible heats of transformation.

Kubashewsky and Catterall (20) give, for up to 33 per cent by weight of copper, the heat of mixing, H_{ML}, of the liquids as

$$H_{ML} = \frac{-9000N_{Cu}}{65.34\ N_{Cu} + 26.98(1-N_{Cu})} \qquad \text{(Eq. 11)}$$

$$N_{Cu} = \frac{26.98C_L}{26.98\ C_L + 63.54(1-C_L)} \qquad \text{(Eq. 12)}$$

The heat of mixing of the solid phases can be considered as a constant. Solid state transformations need not be considered as the transformations are suppressed at these cooling rates. The latent heat of fusion of aluminum is taken as 94.6 cal/gr at 660.2 degrees Celsius and for copper, 50.6 at 1083 degrees.

The thermal conductivity of the alloy can not be calculated easily from the corresponding values of its components, so extrapolation for the different concentrations and temperatures were made from references (18), (19), (20) and (21). The expression used is

$$k = 0.56 + (-2.27 + 4.67\ C_S)C_S - 0.1261 \cdot 10^{-3}(T-25) \qquad \text{(Eq. 13)}$$

and is plotted in Figure 1. Because of the assumption of dendritic growth in the mushy zone, the phases can be considered as resistances in parallel with respect to heat flow, so the overall thermal conductivity for each fraction of the solid present is given as

$$k = f_S k_S + (1 - f_S) k_L \qquad \text{(Eq. 14)}$$

GOVERNING EQUATIONS

The shape of the interfaces between the liquid, mushy and solid zone can be determined from the temperature distribution since definite values of the temperature are associated with them. The Fourier equation of heat conduction

$$\nabla \cdot (k \nabla T) = \rho c \frac{\partial T}{\partial t} \qquad \text{(Eq. 15)}$$

becomes, when symmetry about the axial direction is assumed,

$$\frac{\partial^2 \theta}{\partial r^2} + \frac{\partial^2 \theta}{\partial Z^2} + \frac{1}{r}\frac{\partial \theta}{\partial r} + \frac{\rho c}{k} RU \frac{\partial \theta}{\partial Z} = R^2 \frac{\rho c}{k} \frac{\partial \theta}{\partial t} \qquad \text{(Eq. 16)}$$

where

$$\theta = \frac{1}{K} \int_{T_r}^{T} k(T)\ dT \qquad \text{(Eq. 17)}$$

(K is a constant of proportionality and T_r is a reference temperature)

and, as shown in Figure 2,

$$z = \frac{1}{R}(z' - Ut) \qquad \text{(Eq. 18)}$$

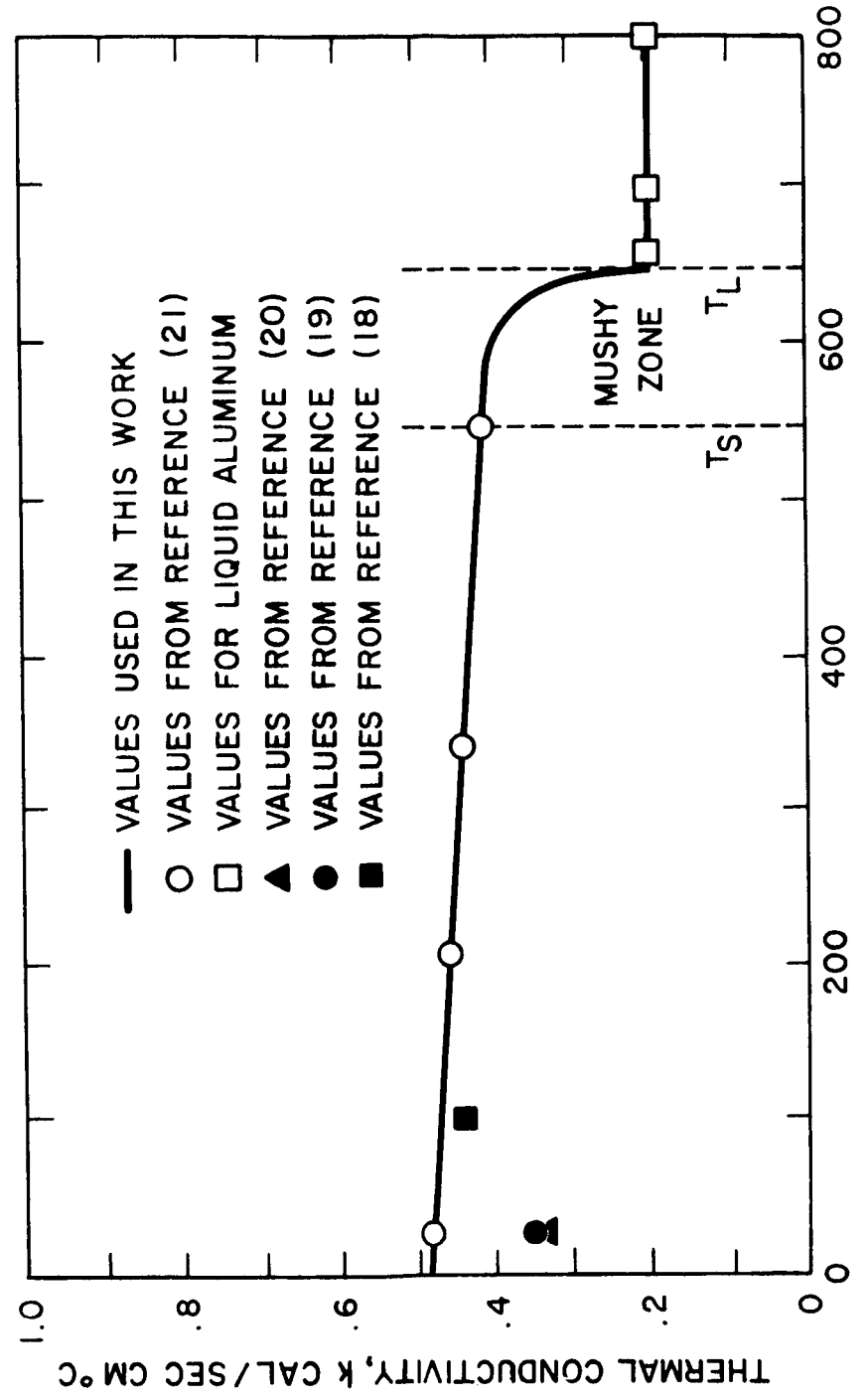

Figure 1 - Thermal conductivity, k, of the Al-5%Cu alloy, versus temperature.

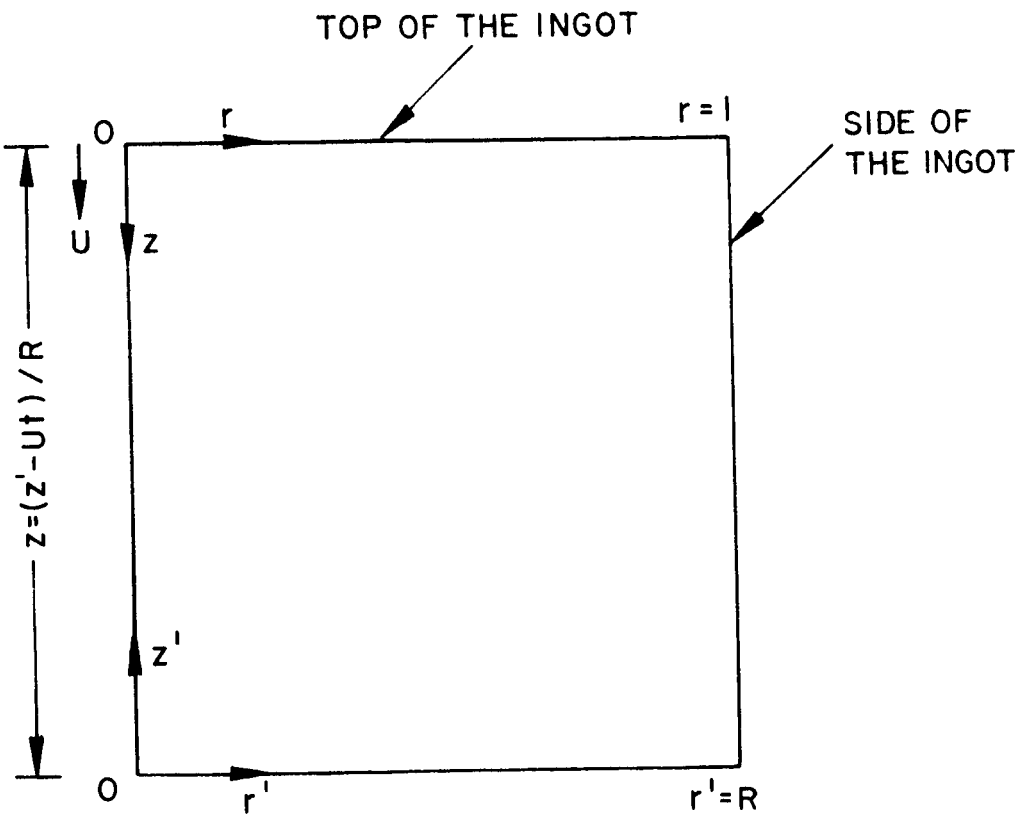

Figure 2 - System of coordinates for growing ingot.

Note that U, the velocity of ingot growth, is a negative value. In equation (16)

$$c = \frac{dH_T}{dT} = f_S \frac{dH_S}{dT} + (1-f_S) \frac{dH_L}{dT} + (H_S-H_L) \frac{df_S}{dT} \quad \text{(Eq. 19)}$$

where $$H_T = f_S(T) \cdot H_S(T) + \left[1-f_S(T)\right] H_L(T) \quad \text{(Eq. 20)}$$

$$H_S = C_S H'_S + (1-C_S) H''_S + H_{MS}(T) \quad \text{(Eq. 21)}$$

$$H_L = C_L H'_L + (1-C_L) H''_L + H_{ML}(T) \quad \text{(Eq. 22)}$$

$$\frac{dH_S}{dT} = C_S c'_S + (1-C_S) c''_S + (H'_S - H''_S) \frac{dC_S}{dT} + \frac{dH_{MS}}{dT} \quad \text{(Eq. 23)}$$

$$\frac{dH_L}{dT} = C_L c'_L + (1-C_L) c''_L + (H'_L - H''_L) \frac{dC_L}{dT} + \frac{dH_{ML}}{dT} \quad \text{(Eq. 24)}$$

Assuming that the solidus and liquidus lines are straight lines, then

$$C_L = (T_M - T) m_L \quad \text{and} \quad C_S = \frac{C_O}{f_S} - \frac{(1-f_S)}{f_S} C_L \quad \text{(Eq. 25)}$$

and its derivative with respect to temperature is

$$\frac{dC_S}{dT} = \frac{C_L-C_S}{f_S} \frac{df_S}{dT} - \frac{1-f_S}{f_S} \frac{dC_L}{dT} \quad \text{(Eq. 26)}$$

Use of Equations (23), (24), (25), along with (11) and (2) permit the evaluation of the derivative of the total enthalpy, equation (19).

BOUNDARY CONDITIONS

At the lateral side of the ingot, r=1, the boundary condition is

$$-k \frac{\partial T}{\partial r} = Rh(T-T_w) \quad \text{(Eq. 27)}$$

where the thermal conductivity, k, of the ingot is evaluated at the ingot surface temperature, T at r=1.

The total heat transfer coefficient, h'is not constant, and must be evaluated, neglecting radiation and convection in the gap between the solidified part of the ingot and mold, by the expression

$$h' = \left(\frac{1}{h_w} + \frac{d_m}{k_m} + \frac{d_g}{k_g} + \frac{d_s}{k_s}\right)^{-1} \qquad \text{(Eq. 28)}$$

where

$$h_w = \frac{k_w}{D_w}\left(\frac{\rho_w V_w D_w}{\mu_w}\right)^{0.8}\left(\frac{c_w \mu_w}{k_w}\right)^{0.33} \qquad \text{(Eq. 29)}$$

A representative value for d_m is one centimeter and for a copper mold, k_m is taken as 0.88 at 400°C. The thickness of the gap d_g is of the order of 10^{-3} cm in continuous casting processes (22). The thermal conductivity of air, k_g, in the gap is 0.14×10^{-3} at 500°C. The ratio $\frac{d_s}{k_s}$ is in the order of 10 considering slag conductivities of 10^{-2}.

To calculate the heat transfer coefficient, h, including radiation inside the gap, the relation derived by Irving (22) is

$$\frac{h-h'}{h} = \frac{\epsilon \sigma d_g T^3}{k_g}\left[\left(1 + \frac{273}{T}\right) + \left(\frac{T_1 - T_w}{T - T_1} + \frac{273}{T}\right)\right]\left[\left(1 + \frac{273}{T}\right)^2 + \left(\frac{T_1 - T_w}{T - T_w} + \frac{273}{T}\right)^2\right] \qquad \text{(Eq. 30)}$$

The emissivity, ϵ, is taken to be 0.5.

The function h versus distance, z, along the lateral sides of the ingot (r=1) used in the analysis is shown on

figure 3. It is assumed that the gap starts forming at temperature, T_S, and from there on an exponential decrease of h with $(z - z_S)$ is considered which corresponds more or less with the exponential growth of the gap and which approximates the trend found by Cliff and Dain (23) in their work for continuous casting.

The boundary condition at the bottom of the ingot, at $z = z_o - Ut$ where z_o is the initial length of the ingot is

$$-k \frac{\partial T}{\partial Z} = Rh(T-T_w) \qquad \text{(Eq. 31)}$$

for the initial transient condition, and which degenerates to $T = T_w$ as the ingot grows and reaches the quasi-steady state condition.

A parabolic temperature distribution for heat generated uniformly inside a cylinder,

$$T = T_{slag} - (T_{slag} - T_L)r^2 \qquad \text{(Eq. 32)}$$

can be applied at the top of the ingot ($z = 0$). A more precise boundary condition would require an investigation of the electric current distribution in the slag.

The temperature at r=1, z=0 is taken as the liquidus temperature, T_L. A lower value would imply a non-uniform growth, while a higher one would require a shifting of the coordinate system to place T_L at the origin, and a modification of the heat transfer coefficient, h, on the lateral side of the ingot.

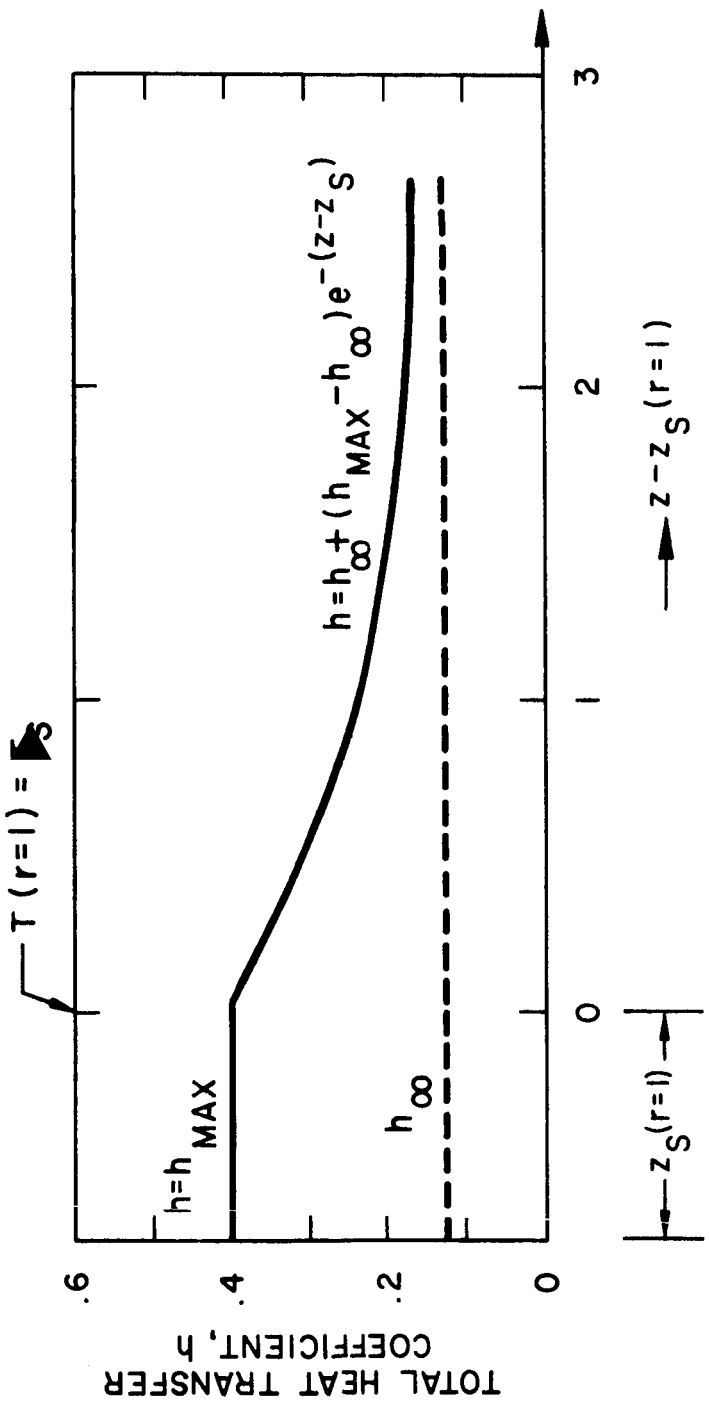

Figure 3 - Total heat transfer coefficient, h, versus axial coordinate of ingot, z.

SOLUTION OF EQUATIONS

An analytical solution was impratical so a finite difference solution was used, the complete details of which are given in reference (24). An important feature of this solution is the introduction of a new transformation of independent variables to extend the region corresponding to the upper portion of the ingot so that a significant number of mesh points are included in the mushy zone without the necessity of using too small a mesh size. This transformation is of the form

$$x = e^{-az} \qquad \text{(Eq. 33)}$$

where a is an appropriately chosen constant. The Alternating Direct Implicit (ADI) method of Peaceman and Rachford (25), was used for the numerical computer solution. The quasi-steady state was reached by iterations on the transient finite difference equations. The ingot lengths were one diameter or less when quasi-steady state was reached. Since the transient temperature distribution is highly dependent on initial temperature distribution, the results of the transient condition are not of significant value from which to draw any conclusions. In the quasi-steady state condition, two significant parameters are

$$K_1 = RU \ (cm^2/sec)$$

$$K_2 = Rh_{max} \ (cal/sec\ cm^{o}C)$$

The overall heat transfer coefficient, h, at the boundary, r=1, will depend on the particular configuration of the mold. A representative value of h_{max} = 0.04 and h_{∞} = 0.0167 (see figure 3) is used here. The numerical values used for K_2 are such that along with h_{max} = 0.04 the ingots are of radius 4, 6, 12, and 24 cm.

For the quasi-steady state condition, which corresponds to an ingot of infinite length, figures 4 to 15 show the shape of the solid and liquid lines determined from the temperature distribution in the ingot for various values of K_1 and K_2, where the slag temperature is assumed to be 644°C, 664°C and 684°C, which correspond to the liquidus temperature of the alloy, 20°C and 40°C superheat, respectively.

Figure 16 shows Q_B, the heat flow distribution at the boundary, r=1, as a function of z for various values of U, for the quasi-steady condition.

$T_{slag} = 644\ °C$

$K_2 = 0.16\ cal/sec\ cm\ °C$

(a) $K_1 = 0.12\ cm^2/sec$

(b) $K_1 = 0.36\ cm^2/sec$

(c) $K_1 = 0.60\ cm^2/sec$

(d) $K_1 = 0.84\ cm^2/sec$

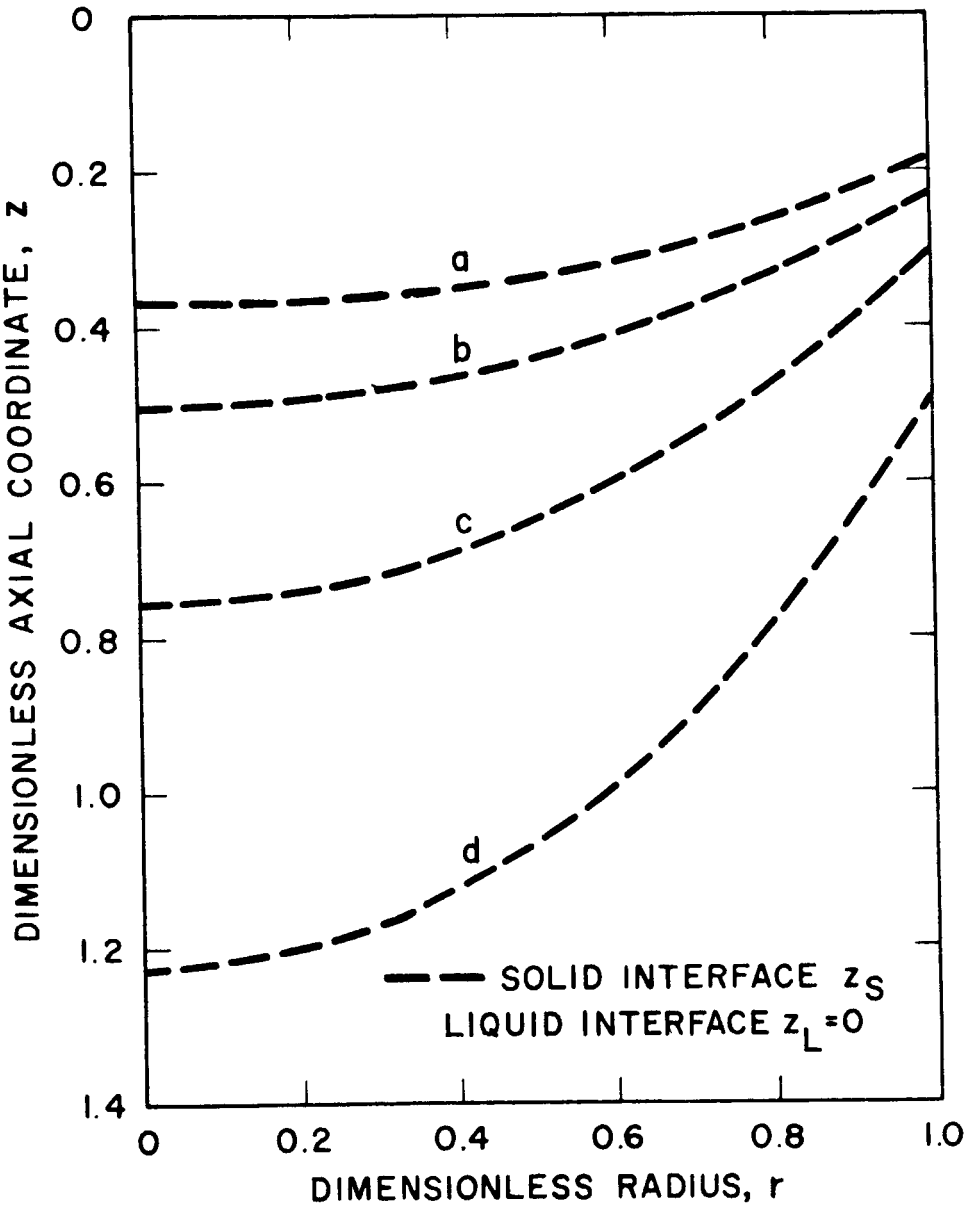

Figure 4 - Solid and liquid interfaces, z_S and z_L, in quasi-steady state.

T_{slag} = 644 °C

K_2 = 0.24 cal/sec cm °C

(a) K_1 = 0.12 cm²/sec

(b) K_1 = 0.36 cm²/sec

(c) K_1 = 0.60 cm²/sec

(d) K_1 = 0.84 cm²/sec

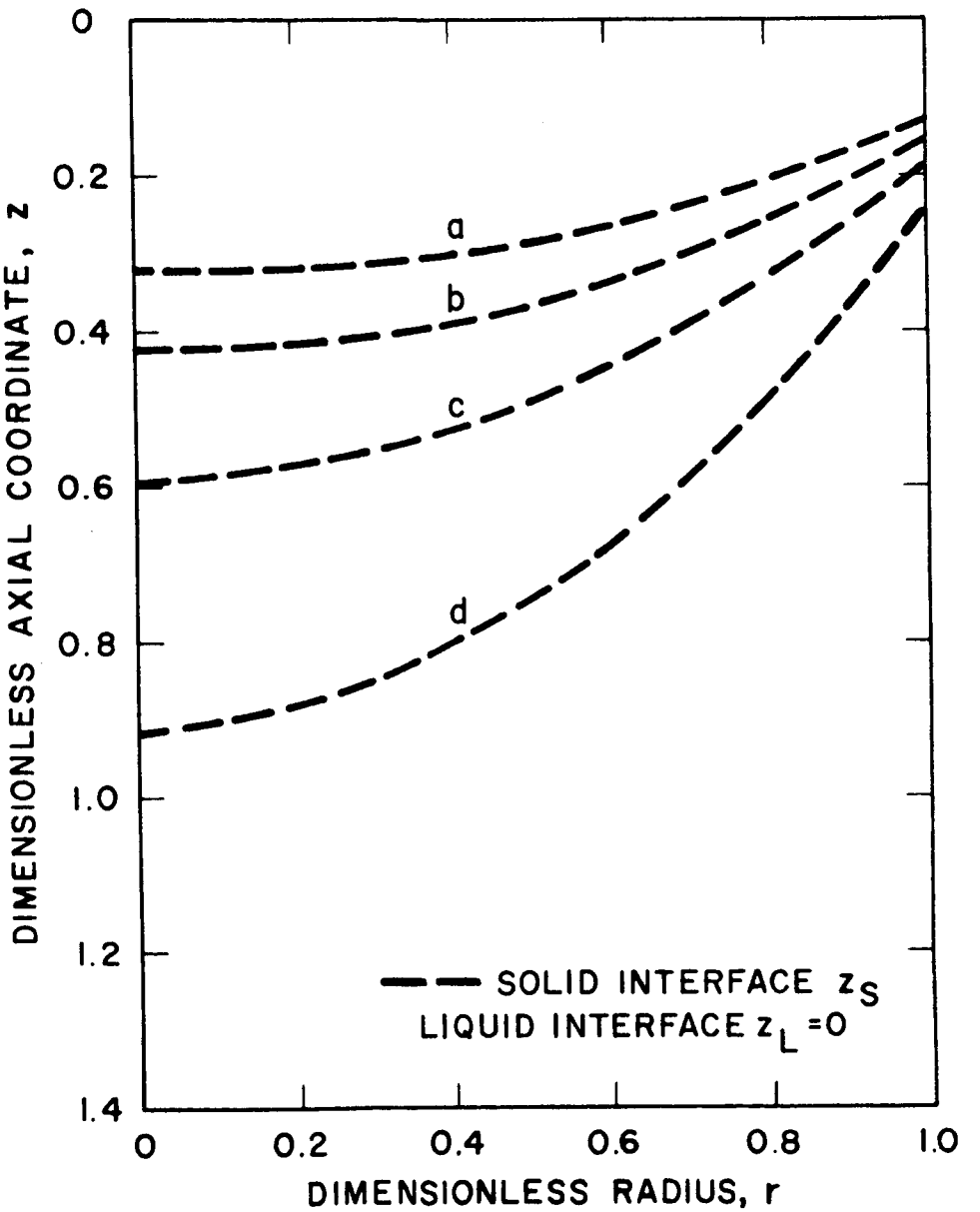

Figure 5 - Solid and liquid interfaces, z_S and z_L, in quasi-steady state.

$T_{slag} = 644\ °C$

$K_2 = 0.48$ cal/sec cm °C

(a) $K_1 = 0.12\ cm^2/sec$

(b) $K_1 = 0.36\ cm^2/sec$

(c) $K_1 = 0.60\ cm^2/sec$

(d) $K_1 = 0.84\ cm^2/sec$

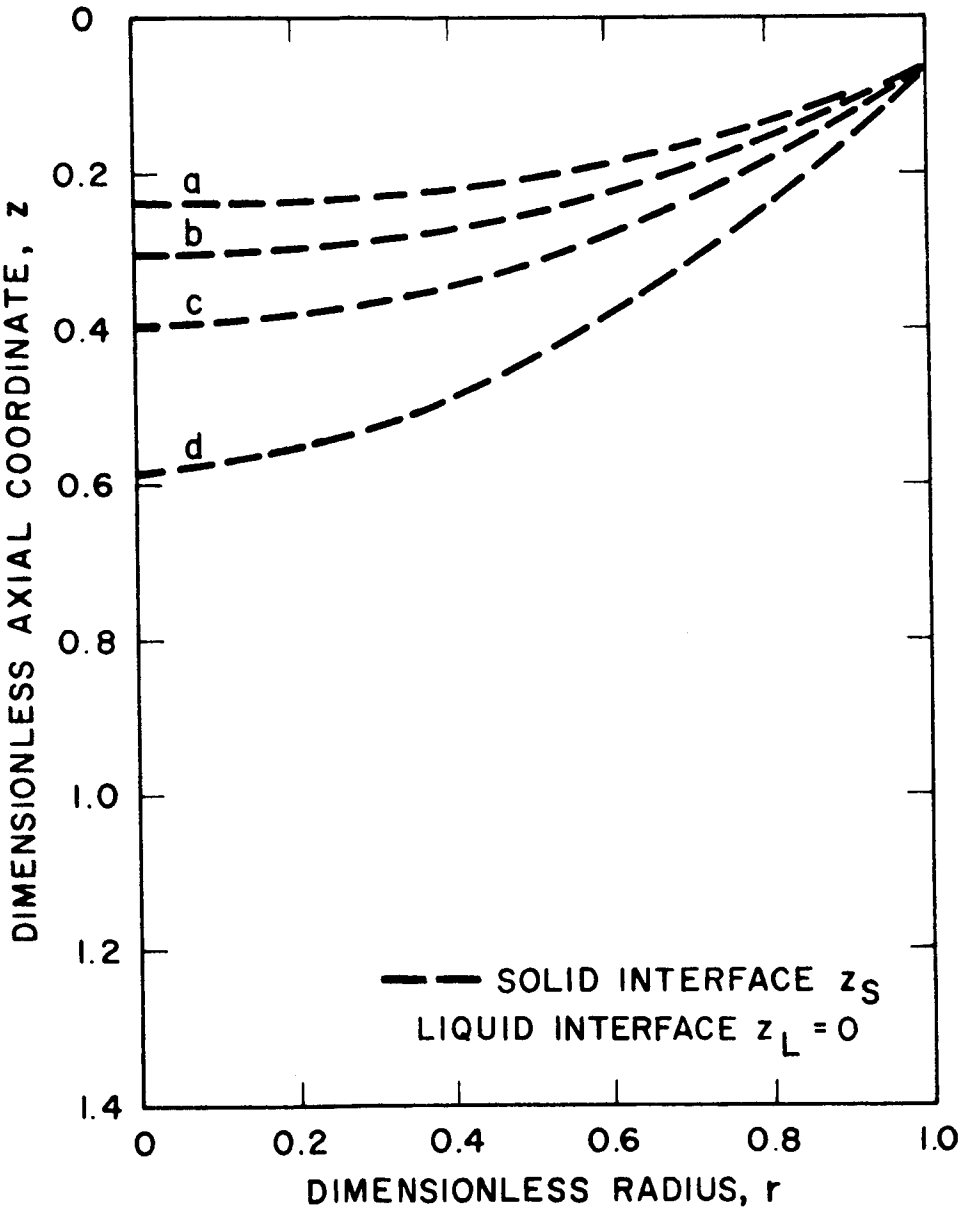

Figure 6 - Solid and liquid interfaces, z_S and z_L, in quasi-steady state.

$T_{slag} = 644\ °C$

$K_2 = 0.96\ cal/sec\ cm\ °C$

(a) $K_1 = 0.12\ cm^2/sec$

(b) $K_1 = 0.36\ cm^2/sec$

(c) $K_1 = 0.60\ cm^2/sec$

(d) $K_1 = 0.84\ cm^2/sec$

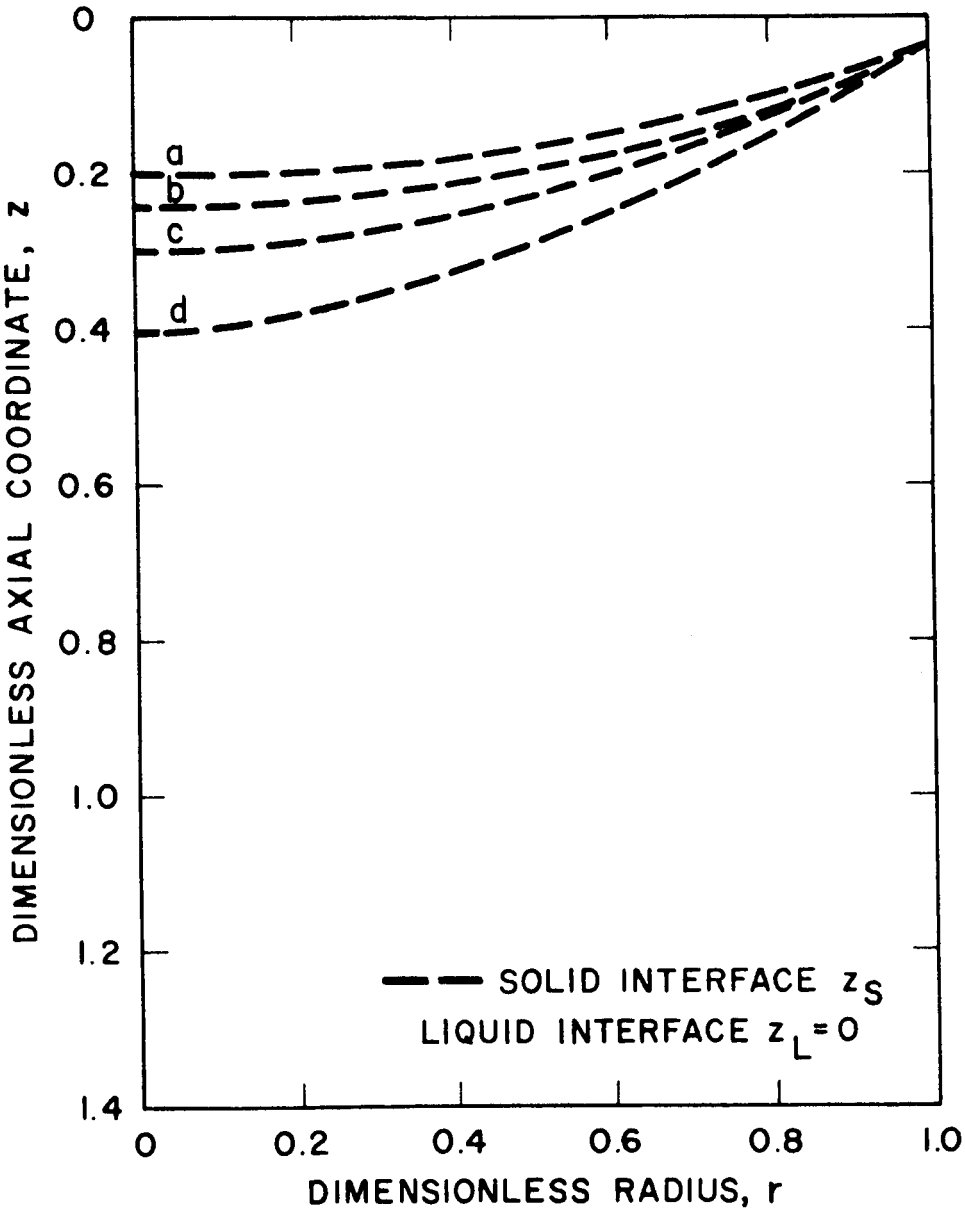

Figure 7 - Solid and liquid interfaces, z_S and z_L, in quasi-steady state.

T_{slag} = 664 °C

K_2 = 0.16 cal/sec cm °C

(a) K_1 = 0.12 cm^2/sec

(b) K_1 = 0.36 cm^2/sec

(c) K_1 = 0.60 cm^2/sec

(d) K_1 = 0.84 cm^2/sec

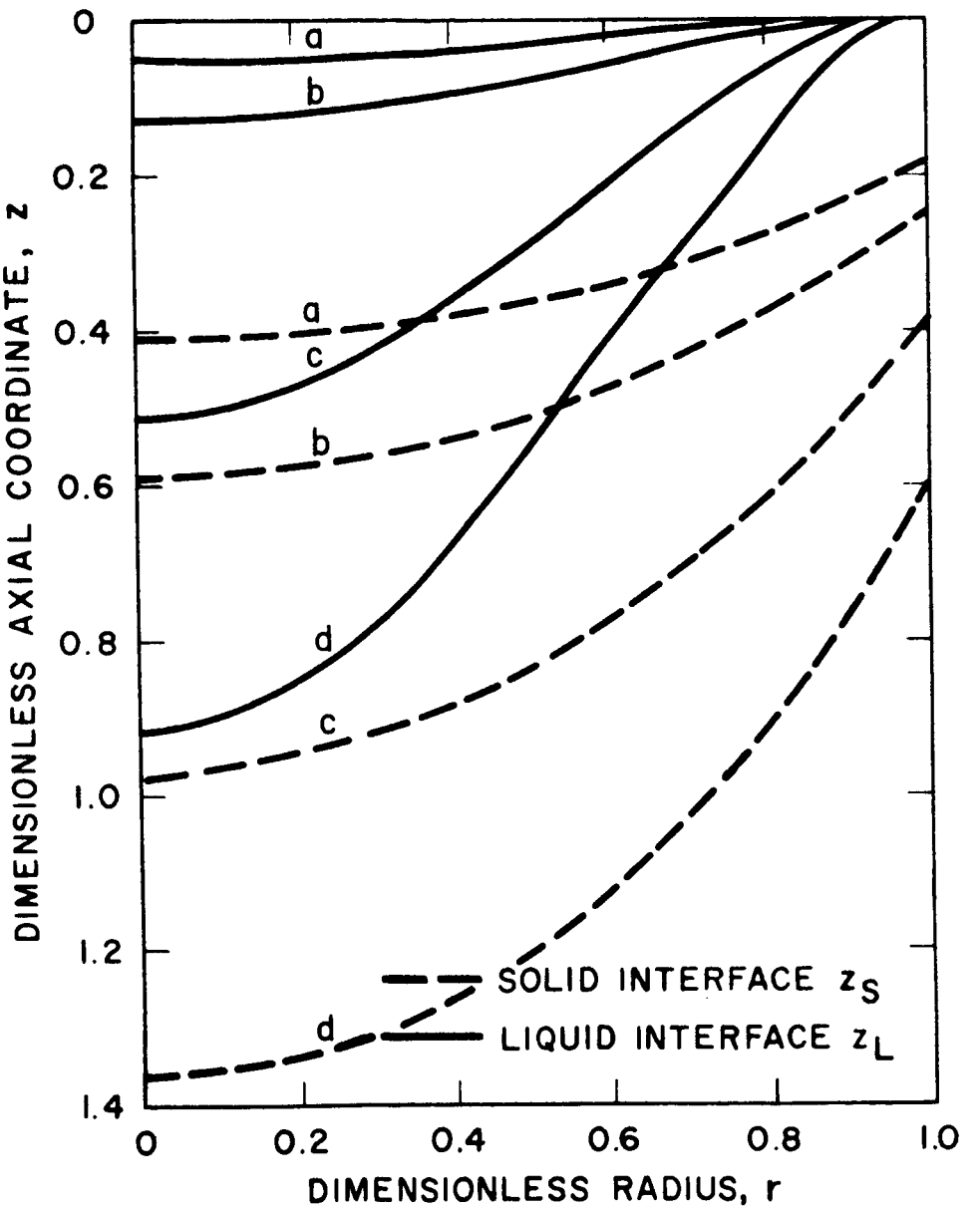

Figure 8 - Solid and liquid interfaces, z_S and z_L, in quasi-steady state.

T_{slag} = 664 °C

K_2 = 0.24 cal/sec cm °C

(a) K_1 = 0.12 cm^2/sec

(b) K_1 = 0.36 cm^2/sec

(c) K_1 = 0.60 cm^2/sec

(d) K_1 = 0.84 cm^2/sec

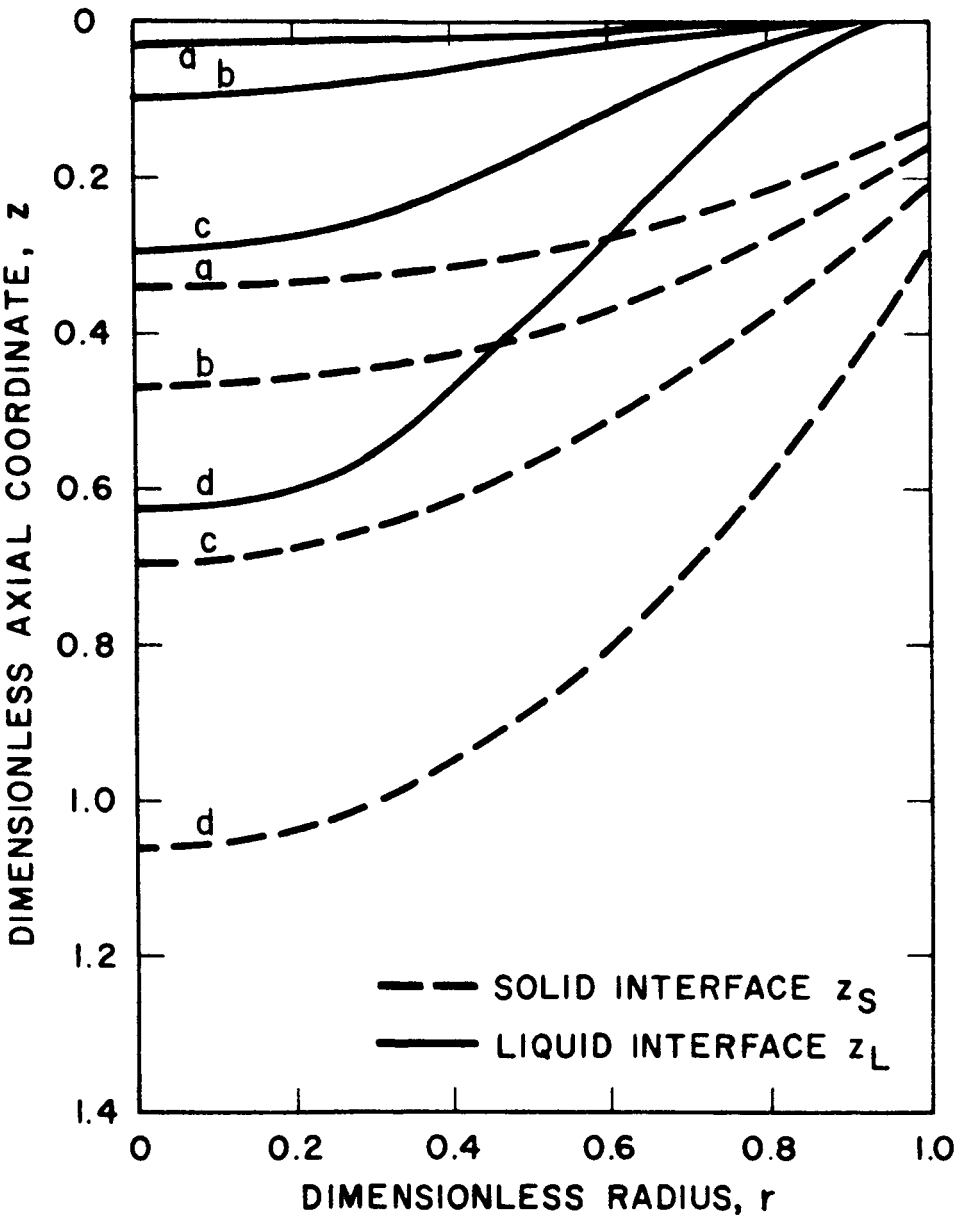

Figure 9 - Solid and liquid interfaces, z_S, and z_L, in quasi-steady state.

T_{slag} = 664 °C

K_2 = 0.48 cal/sec cm °C

(a) K_1 = 0.12 cm^2/sec

(b) K_1 = 0.36 cm^2/sec

(c) K_1 = 0.60 cm^2/sec

(d) K_1 = 0.84 cm^2/sec

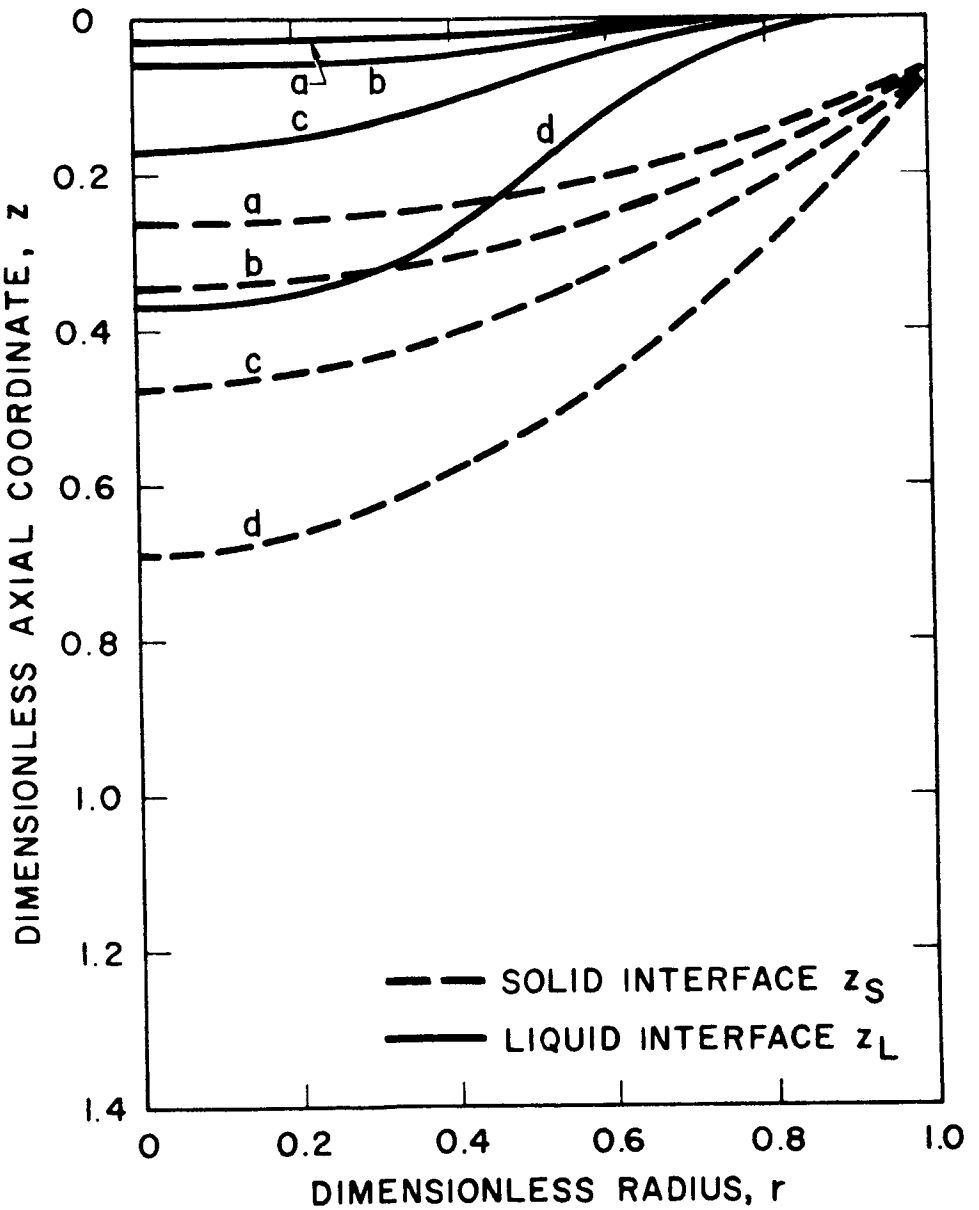

Figure 10 - Solid and liquid interfaces, z_S and z_L, in quasi-steady state.

T_{slag} = 664 °C

K_2 = 0.96 cal/sec cm °C

(a) K_1 = 0.12 cm^2/sec

(b) K_1 = 0.36 cm^2/sec

(c) K_1 = 0.60 cm^2/sec

(d) K_1 = 0.84 cm^2/sec

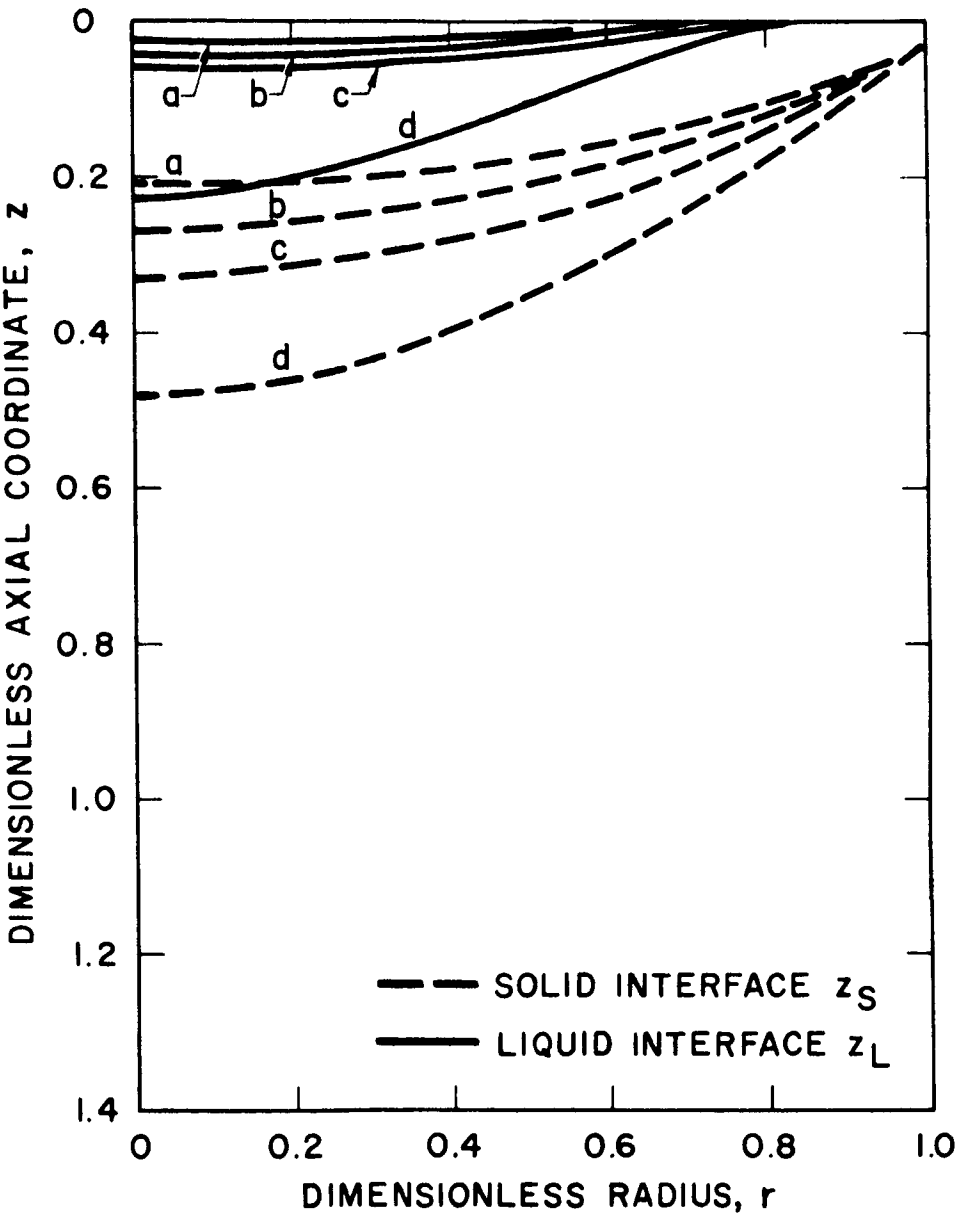

Figure 11 - Solid and liquid interfaces, z_S and z_L, in quasi-steady state.

T_{slag} = 684 °C

K_2 = 0.16 cal/sec cm °C

(a) K_1 = 0.12 cm^2/sec

(b) K_1 = 0.36 cm^2/sec

(c) K_1 = 0.60 cm^2/sec

(d) K_1 = 0.84 cm^2/sec

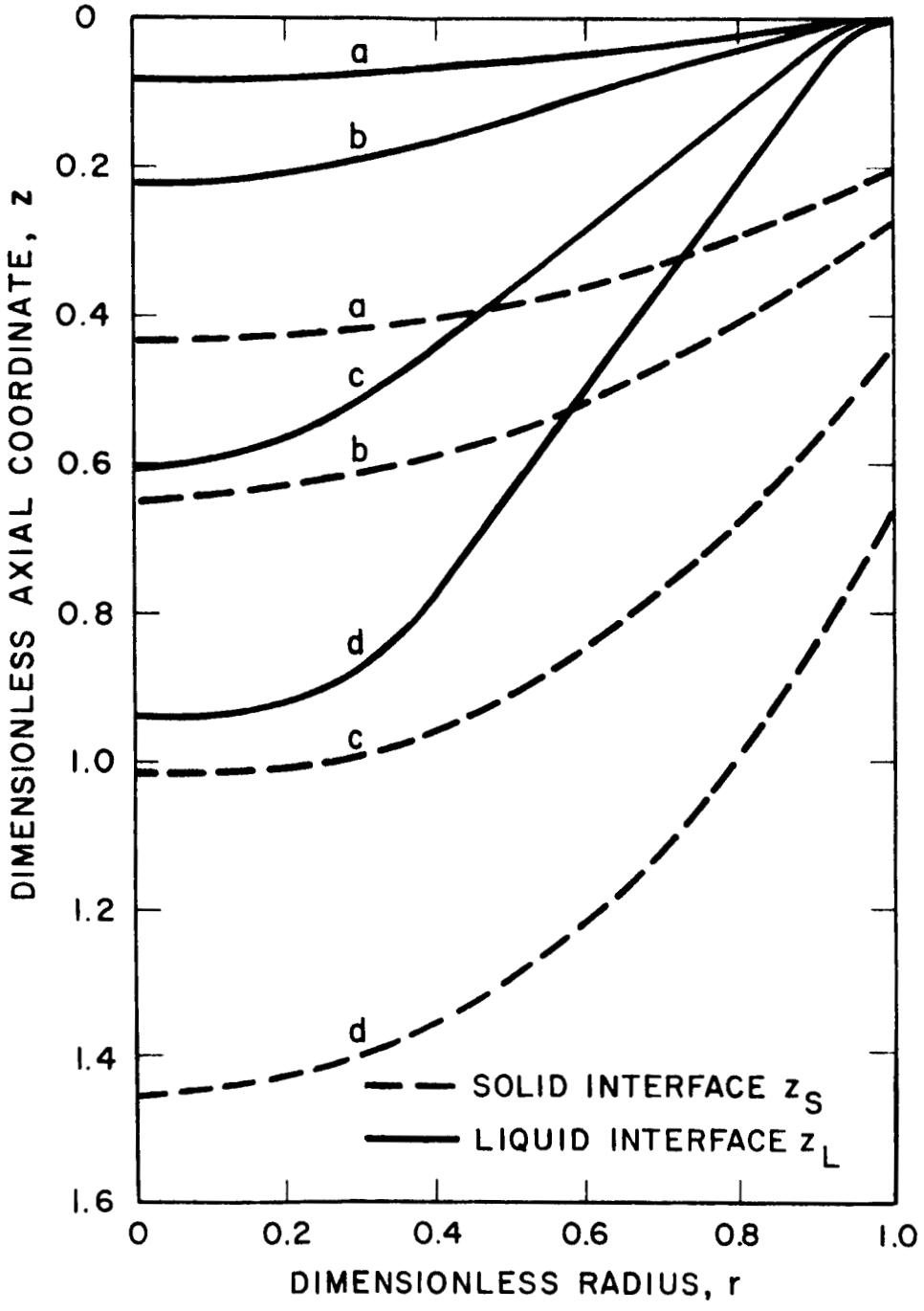

Figure 12 - Solid and liquid interfaces, z_S and z_L, in quasi-steady state.

T_{slag} = 684 °C

K_2 = 0.24 cal/sec cm °C

(a) K_1 = 0.12 cm^2/sec

(b) K_1 = 0.36 cm^2/sec

(c) K_1 = 0.60 cm^2/sec

(d) K_1 = 0.84 cm^2/sec

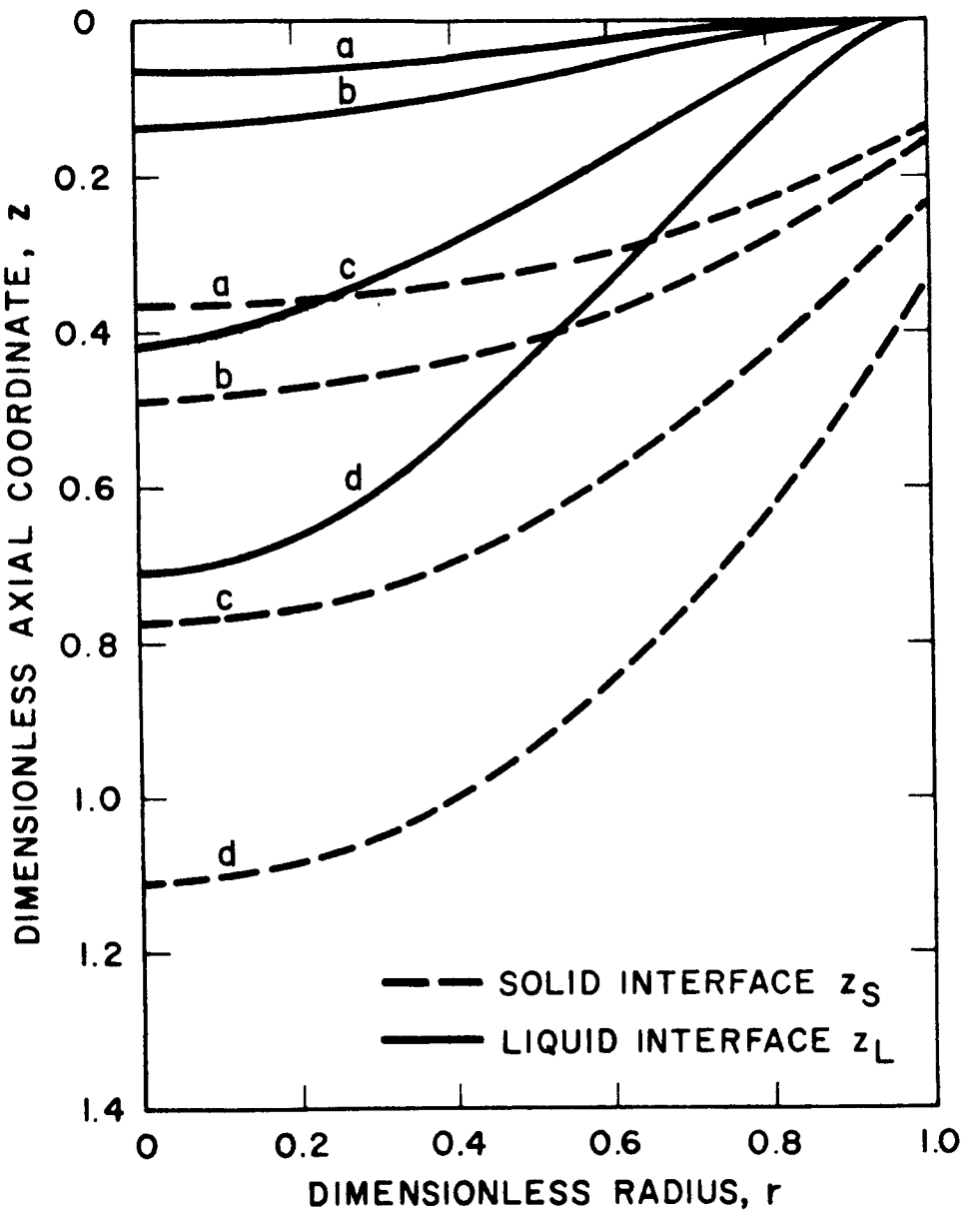

Figure 13 - Solid and liquid interfaces, z_S and z_L, in quasi-steady state.

T_{slag} = 684 °C

K_2 = 0.48 cal/sec cm °C

(a) K_1 = 0.12 cm^2/sec

(b) K_1 = 0.36 cm^2/sec

(c) K_1 = 0.60 cm^2/sec

(d) K_1 = 0.84 cm^2/sec

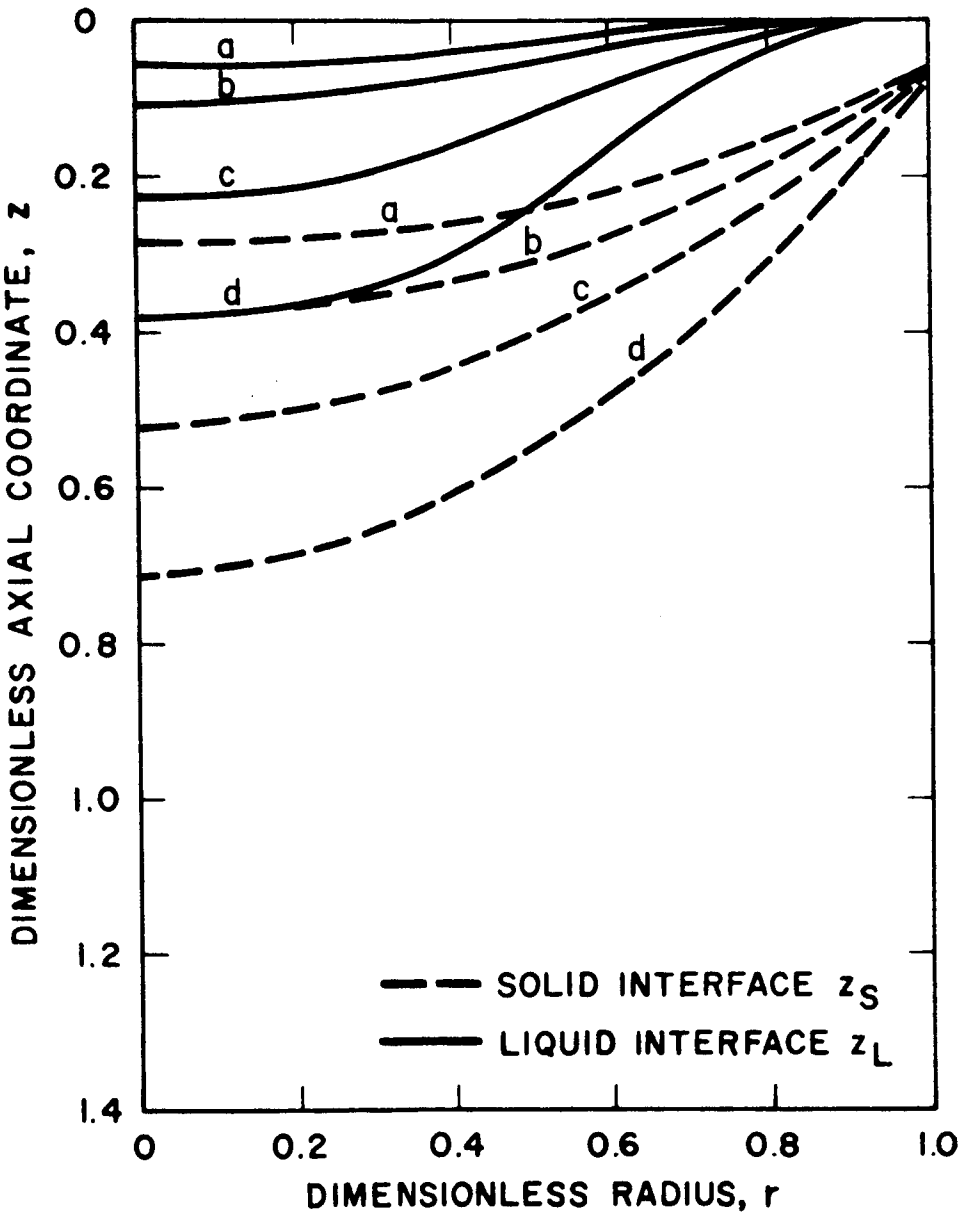

Figure 14 - Solid and liquid interfaces, z_S and z_L, in quasi-steady state.

T_{slag} = 684 °C

K_2 = 0.96 cal/sec cm °C

(a) K_1 = 0.12 cm^2/sec

(b) K_1 = 0.36 cm^2/sec

(c) K_1 = 0.60 cm^2/sec

(d) K_1 = 0.84 cm^2/sec

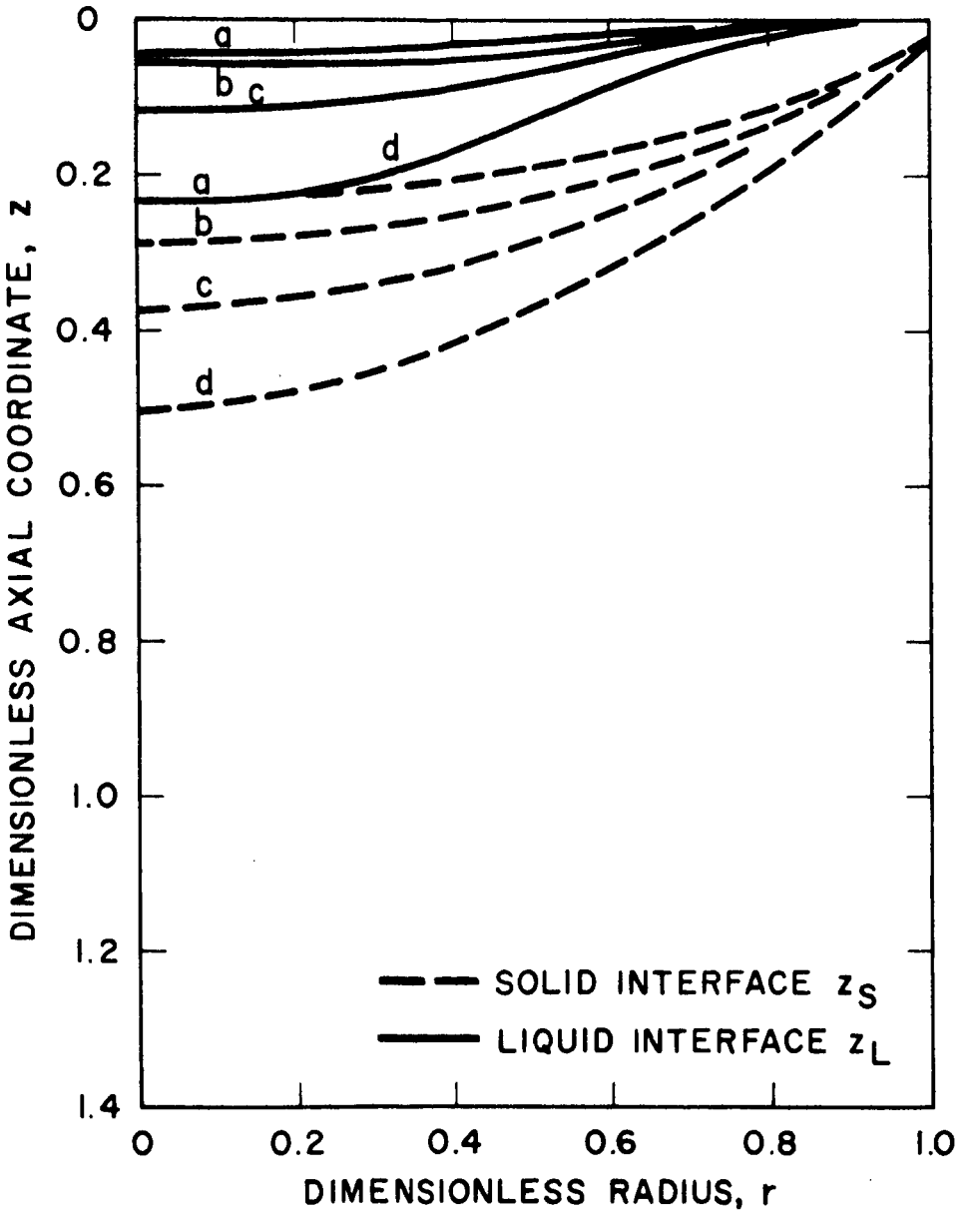

Figure 15 - Solid and liquid interfaces, z_S and z_L, in quasi-steady state.

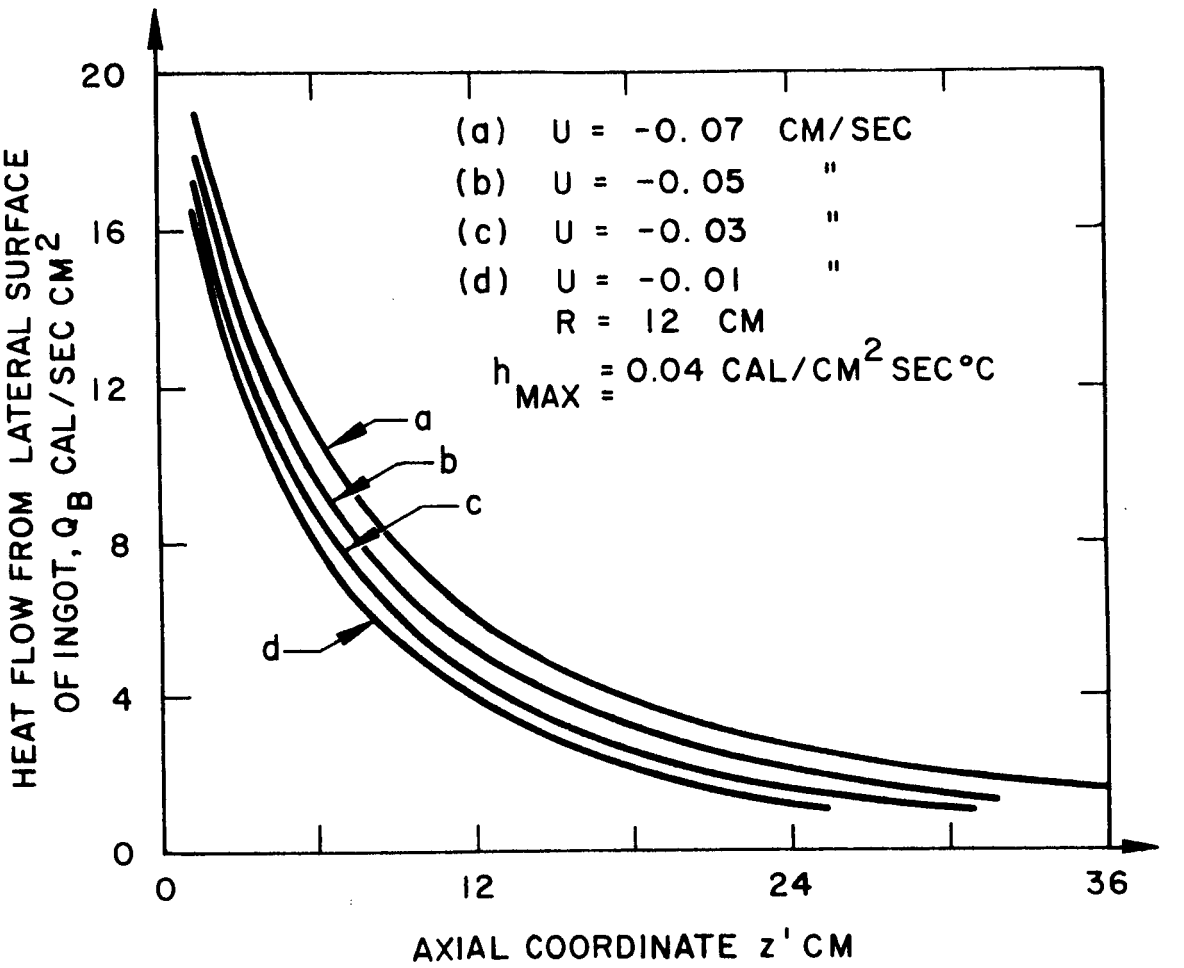

Figure 16 - Heat flow per unit area at the surface r = 1.

CONCLUSIONS

The results show that the influence of superheating on the shape of the mushy zone is not too severe after some superheating exists. This is a favorable factor since the values of T_{slag} are difficult to determine precisely.

A direct comparison with experimental data was not possible due to the lack of information in the literature on the location of the mushy zone in a cylindrical ingot.

Qualitatively the results agree with experimental evidence concerning the shape of the liquid pool (an inverted bell-shape), with the strong dependence of the depth of the pool with the velocity of melting, and with the heat flux distribution to the cooling water.

Figure 17 shows a typical comparison of the shapes of the mushy zone in which the heat release distribution is calculated by the linear heat release model, the parabolic heat release model and the normal non-equilibrium model.

ACKNOWLEDGMENT

The authors wish to acknowledge the aid of Dr. H. Brody, of the University of Pittsburgh, in the metallurgical aspects of this problem. Also we acknowledge the University of Pittsburgh Computational Center, which is partially supported by the National Science Grant No. G-11309, for the use of the computer.

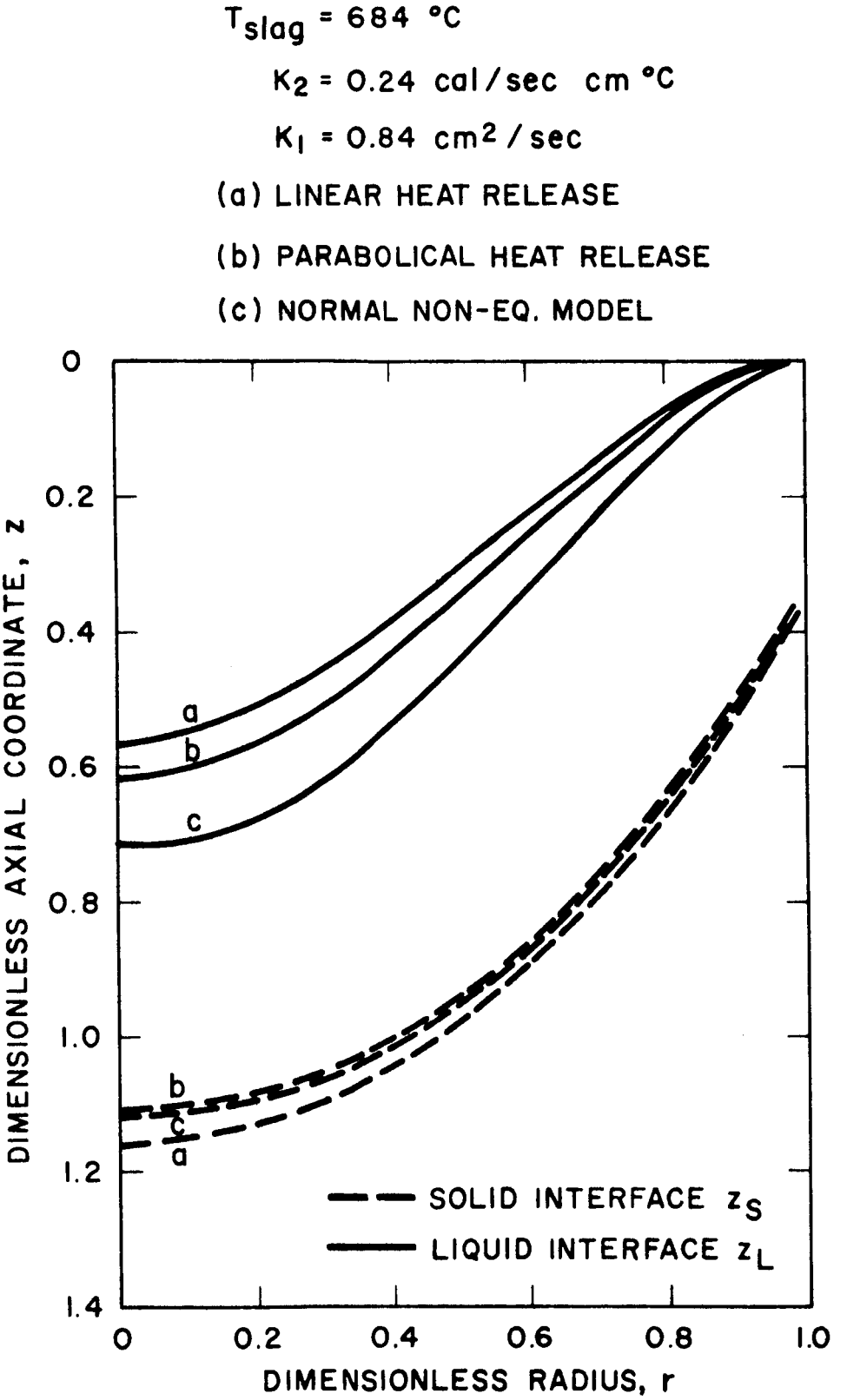

Figure 17 - Comparisons for the shape of the mushy zone for different derivatives dH_T/dT.

BIBLIOGRAPHY

1. Manior, P. du, and Pierce, C. M., "Computer Analysis of the Heat Flow in the Vacuum Arc Melting of Molybdenum," U.S. Air Force Technical Documentary Rept. No. ML-TDR-64-308, October 1964.

2. Wood, F. W., "On the Distribution of Temperature and Heat Flow in Arc Melted Ingots," Oregon State University Thesis, Corvallis, Oregon, 1967.

3. Rossin, P. C., "Arc Melting in High Vacuum," Electrochemical Society Inc., Boston Mass., 1955.

4. Bungardt, Von K. and Tromell, K., "Uber das Schmelzen im Lichtbogen Vakuum Ofen mit Selbstverzehrender Electrode," Archiv fur das Eisenhuttenwesen, page 725, August 1964.

5. Beall, R.A., et. al. "Production of Titanium Castings," U.S. Bureau of Mines, Report of Investigation 5265, 1956.

6. Beall, R. A., Borg, J. O. and Wood, F. W., "A Study of Consumable Electrode Arc Melting," U.S. Bureau of Mines, Report of Investigation 5144, 1955.

7. Patel, P. D., and Boley, B. A. "Solidification Problems with Space and Time Varying Boundary Conditions and Imperfect Mold Contact," International Journal of Engineering Science, Vol. 7, pp. 1041-1066, Pergamon Press, 1969.

8. Tien, R. H., "The Location of the Freezing Zone and the Temperature Distribution for the Solidification Process in a Binary Alloy," Ph.D. Dissertation, University of Pittsburgh, 1966.

9. Tien, R. H. and Geiger, G. E., "A Heat Transfer Analysis of the Solidification of a Binary Eutectic System," ASME Trans. Journal of Heat Transfer, Vol. 89, series c, No. 3, August 1967.

10. Tien, R. H., and Geiger, G. E., "The Unidirectional Solidification of a Binary Eutectic System with a Time-Dependent Surface Temperature," ASME Trans. Journal of Heat Transfer, Vol. 90, series C, No. 1, February 1968.

11. Koump, V., Tien, R. H. and Kim, W. J., "Growth of the Solid and Liquid Region during One Dimensional Solidification of Binary Alloys," Transactions of the AIME, Vol. 279, p.1305, Sept. 1967.

12. Bhat, G. K., "The Technology and Commencial Exploitation Aspects of the Electroslag Remelting Process," First International Symposium on Electroslag Consumable Electrode Remelting and Casting Technology, Mellon Institute, Pittsburgh, August 1967.

13. Clites, P. G. and Beall, R. A., "A Study of Heat Transfer to Water Cooled Copper Crucibles during Vacuum Arc Melting," Bureau of Mines Report 7035, 1967.

14. Pfann, W. G., "Principles of Zone Melting," Transactions of the AIME, p. 747, July 1962.

15. Nero, G. E. and Flemings, M. C., "Effects of the Solidification Variables on the Structure of Aluminum Base Ingots," Casting and Solidification Section, Department of Metallurgy MIT, Contract No. DA-19-020 ORD-5706(A), 1966.

16. Chalmers, B., Principles of Solidification, J. Wiley and Sons, New York, 1964.

17. Van Horn, K. P., ed., Aluminum, Vol. I. American Society for Metals, Metal Park, Ohio, 1967.

18. Metals Reference Book, Fourth Edition, Plenum Press, New York, 1967.

19. American Society of Mechanical Engineers Metals Engineering Handbook Board, ASME Handbook, Vol. 2, Metal Properties, Edited by S. L. Hoyt, McGraw-Hill, New York, 1954.

20. McGraw-Hill Encyclopedia of Science and Technology, McGraw-Hill, New York, 1966.

21. Handbook of Thermophysical Properties of Solid Materials, Goldmith, Waterman and Hirshhorn, MacMillan, 1961.

22. Irving, W. R., "Heat Transfer in Continuous Casting Molds," Iron and Steel Inst. Journal, Vol. 205, p. 271, 1967.

23. Cliff, K. and Dain, R. J., "Computerized Calculations of Operating Conditions in Continuous Casting Machines," Iron and Steel Inst. Journal, Vol. 205, p. 278, 1967.

24. Carvajal, L. F., "Temperature Distribution and Freezing Zone Location in Binary Alloys in Electroslag Remelting," Ph. D. Dissertation, University of Pittsburgh, 1968.

25. Peaceman, D. W. and Rachford, H. H., "The Numerical

Solution of Parabolic and Elliptic Differential Equations," Journal of the Soc. of Indus. and App. Math., Vol. 3, No. 1, 1965.